TOUGHREACT Version 2.0: A Simulator for Subsurface Reactive Transport under Non-isothermal Multiphase Flow Conditions

Tianfu Xu[*], Nicolas Spycher, Eric Sonnenthal, Guoxiang Zhang[†], Liange Zheng, and Karsten Pruess

Earth Sciences Division, Lawrence Berkeley National Laboratory, 1 Cyclotron Road, Berkeley, CA 94720, USA

ABSTRACT. TOUGHREACT is a numerical simulation program for chemically reactive non-isothermal flows of multiphase fluids in porous and fractured media, and was developed by introducing reactive chemistry into the multiphase fluid and heat flow simulator TOUGH2 V2. The first version of TOUGHREACT was released to the public through the U.S. Department of Energy's Energy Science and Technology Software Center (ESTSC) in August 2004. It is among the most frequently requested of ESTSC's codes. The code has been widely used for studies in CO_2 geological sequestration, nuclear waste isolation, geothermal energy development, environmental remediation, and increasingly for petroleum applications. Over the last several years, many new capabilities have been developed, which were incorporated into Version 2 of TOUGHREACT. Major additions and improvements in Version 2 are discussed here, and two application examples are presented, (1) long-term fate of injected CO_2 in a storage reservoir, and (2) biogeochemical cycling of metals in mining-impacted lake sediments.

Key words: Multi-phase flow, Reactive transport, TOUGHREACT, CO_2 geological storage, Environmental remediation, Nuclear waste geological disposal.

[*] Corresponding author; Email address: Tianfu_Xu@lbl.gov (T.Xu).
[†] Current address: Shell International E&P Inc. Houston, TX 77079, USA.

1. Introduction

TOUGHREACT is a numerical simulation program for chemically reactive nonisothermal flows of multiphase fluids in porous and fractured media (Xu and Pruess, 2001; Spycher et al., 2003; Sonnenthal et al., 2005; Xu et al., 2006; Xu, 2008; Zhang et al., 2008; Zheng et al., 2009). The program was written in Fortran 77 and developed by introducing reactive chemistry into the multiphase fluid and heat flow simulator TOUGH2 (Pruess, 2004). The program can be applied to one-, two- or three-dimensional porous and fractured media with physical and chemical heterogeneity. The code can accommodate any number of chemical species present in liquid, gas, and solid phases. A variety of subsurface thermal, physical, chemical, and biological processes are considered under a wide range of conditions of pressure, temperature, water saturation, ionic strength, and pH and Eh.

Processes for fluid flow and heat transport are the same as in the original TOUGH2. Transport of aqueous and gaseous species by advection and molecular diffusion is considered in both liquid (aqueous) and gas phases. Depending on computer memory and CPU performance, any number of chemical species in the liquid, gas, and solid phases can be accommodated. In the 2004 version (Version 1.0) of TOUGHREACT, aqueous complexation, acid-base, redox, gas dissolution/exsolution, and single-site cation exchange were considered under the local equilibrium assumption. Mineral dissolution and precipitation could proceed either subject to local equilibrium or kinetic conditions.

Over the last several years, many new capabilities have been developed within different research projects at Lawrence Berkeley National Laboratory. We have incorporated these new capabilities into Version 2.0 of TOUGHREACT. Major additions and improvements in Version 2.0 include

- Intra-aqueous reaction kinetics and biodegradation,
- Surface complexation models including double layer,
- Multi-site cation exchange,
- Improvements on reactive surface area algorithm for mineral-water reactions, and fugacity coefficient corrections for gas-water reactions,
- Improvements on mineral solid solution model that is an ideal model and only available for minerals reacting under kinetic constraints,

- Improvements in coupling and mass balances between the chemistry and physics parts, including changes in rock and fluid properties due to reactions, and accounting for CO_2 fixed as carbonates in the flow simulation (for using ECO2N module; Pruess and Spycher, 2007).
- Improvement on functionalities such as printouts of mineral reaction rates, and aqueous component and species concentrations in different user-selectable units,
- Improvements in computational efficiency.

TOUGHREACT V2.0 is written in FORTRAN 77 with some Fortran-90 extensions. It has been tested on various computer platforms, including Microsoft Windows- and Linux-based PCs, Apple Macintosh G4 and G5, and Intel-based computers. An effort was made for the TOUGHREACT source code to comply with the ANSIX3.9-1978 (FORTRAN 77) standard, and on most machines the code should compile using Fortran 95, Fortran 90, and some Fortran 77 compilers, and run without modification. TOUGHREACT (like TOUGH2 V2) requires 64-bit arithmetic (8 byte word length for floating point numbers) for successful execution; the code is intrinsically double-precision, to achieve 64-bit arithmetic on the commonly used 32-bit processors. The computer memory required by TOUGHREACT depends on the problem size such as numbers of grid blocks, aqueous and gaseous species, and minerals. Array dimensions are set in parameter statements in INCLUDE files.

The correct implementation, setup, problem formulation, and interpretation of the results of TOUGHREACT requires knowledge of the basic equations of multiphase non-isothermal fluid flow and transport in geologic media, and a basic understanding of the numerical solution of the equations that are used to describe these processes. In addition, the formulation of the geochemical problem requires familiarity with geochemical modeling and an in-depth understanding of the system that is being modeled and of the data used for input to the model. The model boundary conditions, time step length, convergence criteria, and grid properties are crucial elements for a realistic and accurate solution to a problem.

We first present the general formulation for solving flow, transport and reaction equations. To illustrate new features and applicability of TOUGHREACT Version 2, we then present two applications examples.

2. Mathematical Formulation

TOUGHREACT uses a sequential iteration approach similar to Yeh and Tripathi (1991). After solution of the flow equations, the fluid velocities and phase saturations are used for chemical transport simulation. The chemical transport is solved on a component-by-component basis. The resulting concentrations obtained from solving transport equations are substituted into the chemical reaction model. The system of mixed equilibrium-kinetic chemical reaction equations is solved on a grid block by grid block basis by Newton-Raphson iteration. Optionally, the chemical transport and reactions are solved iteratively until convergence. An automatic time stepping scheme is implemented in TOUGHREACT, which includes an option to recognize "quasi-stationary states" (QSS; Lichtner, 1988) and perform a "large" time step towards the end of a QSS.

2.1. Solution of Flow and Transport Equations

The numerical solution of multi-phase fluid and heat flow proceeds as in TOUGH2. Space discretization is made by means of integral finite differences (IFD; Narasimhan and Witherspoon, 1976). Because chemical transport equations (derived from mass conservation) have the same structure as fluid and heat flow equations, the transport equations can be solved by the same numerical method. The basic mass- (for water, air, and chemical components) and energy- (for heat) balance equations are written in integral form for an arbitrary domain with a volume of V_n

$$V_n \frac{\Delta M_n}{\Delta t} = \sum_m A_{nm} F_{nm} + V_n q_n \qquad (1)$$

where subscript n labels a grid block, subscript m labels grid blocks connected to grid block n, Δt is time step size, and M_n is the average mass or energy density in grid block n. Surface integrals are approximated as a discrete sum of averages over surface segments A_{nm}, F_{nm} is the average flux (of mass or energy) over the surface segment A_{nm} between volume elements n and m, and q_n is the average source/sink rate in grid block n per unit volume. Time is discretized fully implicitly as a first-order finite difference to achieve unconditional stability. More detail on the

discretization approach and the definition of the geometric parameters are given in Xu and Pruess (2001) and Pruess (2004). The IFD method gives a flexible discretization for geologic media that allows the use of irregular unstructured grids, which is well suited for simulation of flow, transport, and fluid-rock interaction in multi-region heterogeneous and fractured rock systems. For systems with regular grids, IFD is equivalent to conventional finite differences.

The time discretization of fluid and heat flow equations results in a set of coupled non-linear algebraic equations for the unknown thermodynamic state variables in all grid blocks. These equations are solved by Newton-Raphson iteration as implemented in the original TOUGH2 simulator (Pruess, 2004). The set of coupled linear equations arising at each iteration step is solved iteratively by means of preconditioned conjugate gradient methods.

2.2. Solution of Chemical System

The equations for the chemical system are based on mass balance in terms of primary (basis) species. In contrast to aqueous equilibrium, species involved in kinetic reactions, such as redox couples, are independent and must be considered as primary species (Steefel and MacQuarrie, 1996). For example, for the reaction

$$HS^- + 2O_2(aq) = SO_4^{2-} + H^+ \tag{2}$$

under kinetic conditions, both HS^- and SO_4^{2-} must be placed in the primary species list. Thus, all redox reactions making use of these species must be decoupled in the input of the thermodynamic database.

Details on the formulation for solving the mixed equilibrium-kinetics system of equations are given in Xu (2008). Here we present the final Jacobian equations only. By denoting residuals of mass-balance of each component j as F_j^c (which are zero in the limit of convergence), we have

$$
\begin{aligned}
F_j^c = \ & (c_j - c_j^0) && \text{primary species} \\
& + \sum_{k=1}^{N_x} \nu_{kj}(c_k - c_k^0) && \text{equilibrium aqueous complexes} \\
& + \sum_{m=1}^{N_p} \nu_{mj}(c_m - c_m^0) && \text{equilibrium minerals} \\
& - \sum_{n=1}^{N_q} \nu_{nj} r_n \Delta t && \text{kinetic minerals} \\
& - \sum_{l=1}^{N_a} \nu_{lj} r_l \Delta t && \text{kinetics among primary species} \\
= \ & 0 && j = 1 \ldots N_C
\end{aligned}
\tag{3}
$$

where superscript 0 represents time zero; Δt is the time step; c are concentrations; subscripts j, k, m, and n are the indices of primary species, aqueous complexes, minerals at equilibrium, and minerals under kinetic constraints, respectively; N_c, N_x, N_p, and N_q are the number of corresponding species and minerals; ν_{kj}, ν_{mj}, and ν_{nj} are stoichiometric coefficients of the primary species in the aqueous complexes, equilibrium, and kinetic minerals, respectively; r_n is the kinetic rate of mineral dissolution and precipitation (positive for dissolution and negative for precipitation-units used here are moles of mineral per kilogram of water per time), for which a general multi-mechanism rate law was used (see next section and Appendix A); l is the aqueous kinetic reaction (including biodegradation) index, N_a is total number of kinetic reactions among primary species, and r_l is the kinetic rate which is in terms of one mole of product species per unit time. For product species, the stoichometric coefficients ν_{lj} are positive, for reactant species, they are negative. The expression for r_l is discussed in the next section and presented in Appendix B.

According to mass-action equations, concentrations of aqueous complexes c_k can be expressed as functions of concentrations of the primary species c_j. Kinetic rates r_n and r_l are functions of c_j. (see Appendices A and B). No explicit expressions relate equilibrium mineral concentrations c_m to c_j. Therefore, N_P additional mass-action equations (one per mineral) are needed. Notice that gas dissolution/exsolution, cation exchange, and surface complexation are included in TOUGHREACT, but for simplicity the formulation is not shown here.

2.3. Kinetic Rate Expressions

A multiple mechanism rate law for mineral dissolution and precipitation is employed, which was reported in Xu et al. (2006), and is presented in Appendix A of this paper. A general

rate expression for intra-aqueous kinetic reaction and biodegradation is incorporated into TOUGHREACT, which was given in Xu (2008), and is also presented here in Appendix B.

Temporal changes in porosity and permeability due to mineral dissolution and precipitation can modify fluid flow path characteristics. This feedback between flow and chemistry is considered. Changes in porosity are calculated from changes in mineral volume fractions. Several porosity-permeability relationships are implemented in TOUGHREACT. Details on the formulation are given in Xu et al. (2006).

3. Treatment of Fractured Rock and Heterogeneous Media

3.1. Multiple Interacting Continua

For chemical transport in variably saturated fractured rocks, global fluid flow and transport of aqueous and gaseous species occurs primarily through a network of interconnected fractures, while chemical species may penetrate into tight matrix blocks primarily through relatively slow diffusive transport in gas and liquid phases. Methods developed for fluid flow in fractured rock can be applied to geochemical transport.

The method of "multiple interacting continua" (MINC) is used to resolve "global" flow and transport of chemicals in the fractured rock and its interaction with "local" exchange between fractures and matrix rock. This method was developed by Pruess and Narasimhan (1985) for fluid and heat flow in fractured porous media. The extension of the MINC method to reactive geochemical transport is described in detail by Xu and Pruess (2001). It is well-known that in the case of reactive chemistry, diffusive fluxes may be controlled by reactions occurring near (within millimeters of) the fracture walls. The resolution of concentration gradients in matrix blocks is achieved by appropriate subgridding. The MINC concept is based on the notion that changes in fluid pressures, temperatures, and chemical concentrations propagate rapidly through the fracture system, while invading the tight matrix blocks only slowly. Therefore, changes in matrix conditions will be (locally) controlled by the distance from the fractures and can then be modeled by means of one-dimensional strings of nested grid blocks (Figure 1).

3.2 Multi-Region Model

Similar to "multiple interacting continua" (MINC) for fractured rock, multi-region concepts can be employed in TOUGHREACT for modeling biogeochemical transport in heterogeneous porous media (Gwo et al., 1996; Xu, 2008). The multi-region model was

proposed to account for hierarchical pore structures, the resultant widely distributed pore water velocities, and the effect of local-scale and field-scale heterogeneities on mass transport. Pore regions can either be physically identified as discrete features, or be experimentally determined by separation of water retention curves according to pore classification schemes. Note that the concept of "region" here is not a "regional model" that generally implies a scale measured in square kilometers. The concept being utilized is a sub-REV concept.

An application of the multi-region model was presented in Xu (2008) to denitrification and sulfate reduction (Figure 2). The applicability was evaluated by comparison with column experiments. The matches with measured nitrate and sulfate concentrations were achieved by adjusting the interfacial area between mobile and immobile regions. The match and parameter calibration suggest that TOUGHREACT is not only a useful interpretative tool for biogeochemical experiments, but also can produce insight into the processes and parameters of microscopic diffusion and their interplay with biogeochemical reactions.

The basic idea behind multiple interacting continua or multi-region approaches is to model dispersion by explicitly resolving domains with different advective velocities through appropriate spatial discretization (gridding). This approach is applicable for heterogeneous media in which regions of higher permeability form spatially-extensive correlated structures. Note that hydrodynamic dispersion is not explicitly accounted in TOUGHREACT, which arises from an interplay between non-uniform advection and molecular diffusion. In geologic media, velocities of fluid parcels are spatially variable due to heterogeneities on multiple scales, all the way from the pore-scale to basin-scale. The process is often represented by a Fickian diffusion analog (convection-dispersion equation), which has fundamental flaws and limitations. Details on the dispersion are discussed in Xu and Pruess (2001).

4. Application Examples

TOUGHREACT V2.0 has been applied to a wide variety of geological and environmental problems. An application to denitrification and sulfate reduction was presented in Xu (2008). The possible mobilization of inorganic constituents such as Pb and As in groundwater in response to CO_2 leakage from deep geological storage has been modeled in Zheng et al. (2009), who considered aqueous complexation, mineral dissolution/precipitation, and desorption/adsorption via surface complexation using double layer model. Here, we discuss two examples: (1) long-term fate and transport of injected CO_2 in the storage reservoir using a 2-

D radial flow model; and (2) biogeochemical cycling of iron and other heavy metals (Zn, Pb, Cu) in sediments of Lake Coeur d'Alene, Idaho, which have been heavily impacted by mining activities.

4.1. Long-Term Fate of Injected CO_2

Concern over the consequences of global warming due to increasing levels of anthropogenic carbon dioxide (CO_2) in the atmosphere has led to a variety of proposals to curtail, if not prevent, further increases. One such approach is to inject CO_2, captured from stationary sources (such as fossil-fuel power plants) into deep saline geologic formations. The response of deep formations to CO_2 injection will depend on many factors, including formation permeability and porosity, the presence of heterogeneities such as faults and layers of high or low permeability, the physical and chemical characteristics of the brines, and the nature of the mineral phases that are present. A great deal of specific and detailed information will be required to assess the feasibility of storing CO_2 in a brine formation at any particular site, and to develop engineering designs for CO_2 storage systems. Here, a generic two-dimensional (2-D) radial model applicable to conditions encountered near the Texas gulf coast was used to study the temporal evolution and spatial distribution of the injected CO_2 and the subsequent physical and chemical changes.

Note that new chemical processes added in Version 2.0 were not needed for the modeling this example of geologic CO_2 sequestration (compared to Version 1.0). However, some improvements were used such as in fugacity coefficient corrections for gas-water reactions, in coupling and mass balances between the chemistry and physics parts including changes in rock and fluid properties due to reactions, in accounting for CO_2 fixed as carbonates in the flow simulation, on functionalities of result printouts, and in computational efficiency.

Fluid flow conditions

The 2-D radial model was a sandstone formation of 40 m thickness with a cylindrical geometrical configuration (Figure 3). The hydrogeological parameters used are listed in Table 1, the formation was assumed as homogenous initially. The petrophysical characteristics such as porosity and permeability were taken from the storage formation of the upper C sandstone of the Frio CO_2 test site (Hovorka et al., 2006; Doughty et al., 2008). The vertical permeability is one order of magnitude smaller than the horizontal one. A hydrostatic pressure distribution over the

depth was specified initially. The shale caprock was assumed impermeable and non-reactive for the present study of coupled processes in the storage reservoir. We did not use the geometry of the Frio Pilot test flow model, because the reservoir is only 5.5 m thick and only 1600 t of CO_2 were injected (Freifeld et al., 2005), which may not represent a realistic CO_2 storage reservoir conditions.

For numerical simulation, in the vertical direction a total of 20 model layers were used with a constant spacing of 2 m. In the horizontal direction, a radial distance of 100 km was modeled with a radial spacing that increases gradually away from the injection well. A total of 56 radial grid elements were used. The volume of the outer grid element is specified a large value of 10^{30} m^3, representing an infinite lateral boundary for constant pressure, temperature and concentrations. CO_2 injection was applied at the bottom portion over 8 m thickness with a constant rate of 20 kg/s (corresponding to 0.64 Mt/year) for a period of 10 years. Our 2-D radial model of fluid flow and geochemical transport was simulated for a period for 1,000 years, which is a relevant time scale for CO_2 geological sequestration. We considered a system with initially homogeneous porosity and permeability. Changes in porosity and permeability due to mineral alteration will seed fluid dynamics instabilities and promote convective mixing.

Geochemical system

The initial rock mineralogical composition was taken from Xu et al. (2007), which may be representative of US Gulf Coast sandstone formations (Table 2). Calcite was assumed to react with aqueous species at local equilibrium because its reaction rate is typically quite rapid. Dissolution and precipitation of other minerals are kinetically-controlled. A multiple mechanism rate law is used, which is given in Appendix A. Kinetic parameters are the same as in a previous study (Xu et al., 2007), and are given in Appendix B.

The initial water chemical composition (Table 3) represents a NaCl-dominated brine of a sample from the Frio test site (Kharaka et al., 2009). A temperature of 75°C was used throughout, which may represent temperature at a depth of about 2 km, given a land surface temperature of 15°C and a geothermal gradient of 30°C/km. Prior to simulating reactive transport, batch geochemical modeling of water-rock interaction was performed to equilibrate the measured chemical composition with the primary minerals listed in Table 2 at a CO_2 gas pressure of 0.1 bar and a temperature of 75°C. The background (initial) CO_2 gas pressure was chosen to match the measured pH. A reasonably short simulation time (10 years in the present study) is needed to obtain nearly steady-state aqueous solution composition for the reactive transport simulation. In

our previous studies such as in Xu et al. (2007), the initial water chemistry for reactive transport simulation was obtained using the same procedure, but starting from a solution of 1 M NaCl with very low concentrations for other aqueous components, because Frio water sample was not available when the previous simulation was performed.

Results and discussion

The supercritical CO_2 fluid (called "gas" here for simplicity) injected near the bottom of the storage formation migrates upward rapidly by buoyancy forces because the density of supercritical CO_2 phase is lower than that of aqueous phase (Figure 4). A small fraction of CO_2 gas is trapped in the porous rock as residual gas after injection. The residual gas trapping keeps CO_2 dissolving into brine and precipitating carbonate minerals, and gradually disappears at the bottom of the reservoir. Over time most of the free CO_2 gas accumulates below the caprock, and then spreads laterally. To about 60 m radial distance rock pores are completely filled by CO_2 gas at 10 years (complete water drying out zone). After injection ends (at 10 years), groundwater re-invades previously dried-out zones and chemical reactions (dissolution and precipitation) between the dissolved CO_2 and minerals proceed.

The simulated total dissolved CO_2 concentrations after 1000 yr are presented in Figure 5a. With the migration of CO_2 gas, the concentration of dissolved CO_2 rapidly increases to larger than 1 mol/kg H_2O in the two-phase region. The injected CO_2 is dissolved in the surrounding formation water, forming H_2CO_3, HCO_3^-, and CO_3^{2-}, and decreasing pH. Then, the increased acidity induces dissolution of many of the primary host rock minerals (discussed later). The mineral dissolution increases concentrations of cations such as Na^+, Ca^{2+}, Mg^{2+}, and Fe^{2+}, which in turn form aqueous complexes with the bicarbonate ion such as $NaHCO_3$, $CaHCO_3^+$, $MgHCO_3^+$, and $FeHCO_3^+$. Over time they tend to increase dissolved CO_2 (solubility) and enhance solubility trapping. Figure 5a shows a "fingering" flow patterns near the bottom of the CO_2 plume. This arises from advection in the aqueous phase that is triggered by an increase in density due to CO_2 dissolution.

Minerals such as oligoclase and chlorite dissolve in the two-phase region and near the front of the single aqueous-phase zone, supplying reactants for carbonate mineral precipitation. Some amount of siderite (Figure 6a), and significant amount of ankerite (Figure 6b) precipitate, sequestering injected CO_2 (mineral trapping). At the same time, clay minerals such as smectite-Na precipitate.

Changes in porosity are calculated from variations in mineral volume fractions. Porosity increases slightly in the two-phase region due to dominant mineral dissolution (Figure 7) caused by low pH. In contrast, porosity decreases at the front of the aqueous-phase because of higher pH and carbonate mineral precipitation. A simple cubic Kozeny-Carman grain model was used to calculate associated changes in permeability. The pattern of permeability change is similar to that of porosity.

Evolution of amounts of CO_2 stored in the three phases over time is presented in Figure 8. During the CO_2 injection period (0-10 years), a large amount of injected CO_2 remains as a free supercritical phase. After the stop of injection, the mass of CO_2 dissolved in the formation water gradually increases because of the upward and horizontal migration of CO_2 plume and the convective mixing between CO_2-saturated water and unsaturated water. CO_2 mineral trapping starts at about 50 years when primary mineral dissolution has neutralized the pH, and subsequently increases gradually (almost linearly) with time. After 1,000 years, 43% of the injected CO_2 is stored in the gas phase, 28% in the aqueous, and 29% in the solid (mineral) phase.

As discussed in Xu et al. (2007), the modeling provides valuable insights regarding the physical and chemical consequences of CO_2 injection in the subsurface environment. Note that the results are constrained by parameter uncertainties. Mineral alteration and CO_2 trapping capability depend on the primary mineral composition. Precipitation of siderite and ankerite requires Fe^{2+}, which can be supplied by the dissolution of iron-bearing minerals, such as chlorite, or by reduction of Fe^{3+} in small amounts of hematite. Variation in Ca content in plagioclase significantly affects carbonate mineral precipitation, and thus CO_2 mineral trapping. The time required for mineral alteration and CO_2 sequestration depends on the rates of mineral dissolution and precipitation.

If carbon dioxide stored in deep saline aquifers were to leak into an overlying aquifer containing potable groundwater, the intruding CO_2 would change the geochemical conditions and cause secondary effects mainly induced by changes in pH. In particular, hazardous trace elements such as lead and arsenic, which may be present in the aquifer host rock, could be mobilized. TOUGHREACT Version 2.0 has been used to evaluate the potential risks to potable water quality by analyzing mechanisms through which lead and arsenic might be mobilized by intrusion of CO_2 (Zheng et al., 2009). The chemical reactions considered by Zheng et al. include aqueous complexation, mineral dissolution/precipitation, and desorption/adsorption via surface complexation using double layer model. Simulation results indicate that desorption/adsorption

could be the most important process controlling the fate of hazardous trace elements mobilized by CO_2 leakage when sorbing minerals are present. The relative importance of dissolution/precipitation versus desorption/adsorption is controlled by many factors, including sorption parameters and aquifer mineralogy, reaction kinetics, aqueous complexation processes, and mineral solubility constants.

4.2. Biogeochemical Cycling of Metals in Mining-impacted Lake Sediments

This example builds on the work presented by Sengör et al. (2007a,b) on modeling the diffusive transport of heavy metals (Zn, Pb, Cu) in the sediments of Lake Coeur d'Alene, Idaho. Details on the conceptual model and implemented biogeochemical reaction network are given in Sengör et al. (2007a,b) and summarized below.

The sediments of Lake Coeur d'Alene have been heavily impacted by mining activities and, as a result, contain elevated concentrations of iron and heavy metals. These sediments contain significant amounts of iron hydroxides, primarily as ferrihydrite (Toevs et al., 2006; Moberly et al. 2009), together with quartz and siderite as major minerals. The microbial reductive dissolution of iron hydroxides in the sediments is thought to lead to the release of metals sorbed onto these mineral phases, generating benthic fluxes of metals from the sediments to the lake water (Balistrieri, 1998; Kuwabara et al., 2003). Deeper into the sediments, metals mobilized by reductive dissolution become immobilized by reaction with biogenic sulfide to form sulfide minerals. These coupled processes are simulated for a 1D sediment column under redox disequilibrium conditions (Figure 9).

The model setup and input data are essentially unchanged from the model presented earlier (Sengör et al. 2007b), which was built using PHREEQC (Parkhurst and Appelo, 1999). The model incorporates a multicomponent biotic reaction network with multiple terminal electron acceptors (TEA) (Table 4), diffusive transport, mineral precipitation and dissolution, and surface complexation. The switch from one TEA to the next is implemented using inhibition factors (K^{in} in Table 4) in the manner proposed by Van Cappellen and Gaillard (1996). We have added to the original 1-D model the effect of sedimentation, approximated by advecting sediment solids and pore water downward at a rate decreasing with depth to mimic compaction. In addition to species originally considered for sorption onto Fe hydroxides (Zn^{2+}, Cu^{2+}, Cu^+, Pb^{2+}, H^+, Ca^{2+}, Mg^{2+}, SO_4^{2-}; Dzombak and Morel, 1990), Fe^{2+} surface complexation (Liger et al., 1999) was also added to the original model. Note that rate laws for the various biotic reactions

(Table 4) are multiplied by a thermodynamic affinity term $(1 - Q/K)$, where Q and K are the ion activity product and the equilibrium constant, respectively, of the reaction) that effectively shuts down the reaction if/when equilibrium is reached (at which point $Q = K$).

The top model boundary is located at the lake water-sediment interface. It is set at a fixed composition equal to the (measured) composition of lake water equilibrated with sorption sites on ferrihydrite. Transport is entirely diffusive, with a closed bottom model boundary. The simulated 1D sediment column is 45 cm long, with a grid spacing of 0.5 cm for the first top 8 cells, then increasing to 1 cm through the remainder of the column. The sedimentation rate is set at 2 cm/yr at the top of the column (Horowitz et al., 1995), and linearly decreasing to zero at the base of the column. The diffusion coefficient is low ($\sim 4 \times 10^{-6}$ cm^2/s), reflecting very fine-grained sediments (Balistrieri, 1998). Simulations are carried out for a period of about 5 years, after which nearly steady conditions prevail.

The same aqueous reaction network is modeled as in Sengör et al. (2007b) (Tables 4 and 5). Higher in the sediment column, iron-reducing bacteria reduce iron hydroxides:

$$8Fe(OH)_{3(s)} + CH_3COO^- + 15H^+ \rightarrow 8Fe^{2+} + 2HCO_3^- + 20H_2O \qquad (4)$$
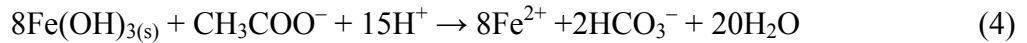
This reaction leads to the release of sorbed metals (Zn, Cu, Pb). At depth, sulfate reducing bacteria produce sulfide, which can react with Fe(II) and other metals to form precipitates:

$$Fe^{2+} + CH_3COO^- + SO_4^{2-} \rightarrow FeS_{(s)} + 2HCO_3^- + H^+ \qquad (5)$$
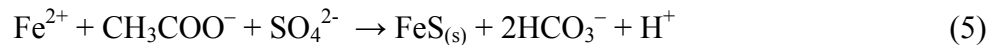
Reactions (4) and (5) represent overall reactions that proceed though the coupling of the reaction network (Table 4) with ferrihydrite (modeled as $Fe(OH)_3$) and mackinawite (FeS, disordered) reacting at equilibrium. Sphalerite (ZnS), galena (PbS) and chalcocite (Cu_2S) are included as "proxy" phases precipitating under kinetic constraints to provide a sink for heavy metals. Siderite ($FeCO_3$) is also included as a phase reacting under kinetic constraints. The only minerals initially present in the modeled column are ferrihydrite and siderite, which are observed throughout the lake sediments in significant amounts (Toevs et al., 2006), likely from both detrital and diagenetic origins (Table 6).

Simulations are started with (oxic) lake water (Table 7) initially throughout the column. A redox stratification eventually develops through the microbial reaction network (Table 4), from oxic lake-water conditions at the top of the column to sulfate-reducing conditions at the

bottom of the column. Kinetic reaction parameters are initially obtained from the literature, then are adjusted as necessary to best match the model results to field data (Winowiecki, 2002) (Figure 10). Note that the electron donor is taken as acetate, which is reported in pore water at ~150 μM and is assumed un-limiting.

Modeled concentration trends for key species are generally consistent with measured data (Figure 10). The behavior of heavy metals is driven by desorption at shallow depth, accompanied by the microbial reductive dissolution of ferrihydrite, and precipitation with biogenic sulfide deeper into the sediment column. In the present case, the precipitation rates of heavy metal sulfides are kept relatively low and roughly adjusted to yield metal concentrations within the observed range. A delicate balance is predicted between the competition of FeS and $FeCO_3$ precipitation for Fe(II), and the competition of soluble (bi)sulfide complexes and sulfide mineral precipitation for biogenic sulfide. Results compare well with the original PHREEQC model developed by Sengör et al. (2007b), with small differences resulting from processes added to the original model, namely Fe(II) sorption onto ferrihydrite and sedimentation, and differences in the affinity terms on the kinetic rate laws of minerals (Table 6). This example provides a typical application of TOUGHREACT V2.0 to a complex reaction network in a shallow, low-temperature environmental system at redox disequilibrium.

5. Conclusions

A non-isothermal reactive transport program, TOUGHREACT, has been developed, which allows comprehensive modeling of chemical interactions between liquid, gaseous and solid phases that are coupled to solute transport and subsurface multiphase fluid and heat flow. The program is applicable to one-, two-, or three-dimensional geologic domains with physical and chemical heterogeneity, and can be applied to a wide range of subsurface conditions of pressure, temperature, water saturation, ionic strength, and pH and Eh. The program can be applied to a variety of problems, including contaminant transport and environmental remediation, natural groundwater quality evolution under ambient conditions, assessment of nuclear waste disposal sites, sedimentary diagenesis and CO_2 sequestration in deep saline formations, mineral deposition such as supergene copper enrichment, and mineral alteration and silica scaling in hydrothermal systems under natural and production conditions.

The examples discussed in this paper demonstrate that TOUGHREACT is a useful tool for modeling non-equilibrium physical and chemical processes in natural or engineered

subsurface systems. Important challenges remaining for future research include consistent thermodynamic and kinetic data, ion activity models for conditions with high ionic strength fluids, description of rock-fluid interactions in the absence of an aqueous phase.

Acknowledgment

Appendix A. Kinetic rate law for mineral dissolution and precipitation

The general rate expression used in TOUGHREACT is taken from Lasaga et al. (1994):

$$r_n = \pm k_n A_n \left| 1 - \left(\frac{Q_n}{K_n} \right)^{\theta} \right|^{\eta} \tag{A.1}$$

where n denotes kinetic mineral index, positive values of r_n indicate dissolution, and negative values precipitation, k_n is the rate constant (moles per unit mineral surface area and unit time) which is temperature dependent, A_n is the specific reactive surface area per kg H_2O, K_n is the equilibrium constant for the mineral-water reaction written for the destruction of one mole of mineral n, and Q_n is the reaction quotient. The parameters θ and η must be determined from experiments; usually, but not always, they are taken equal to one.

For many minerals, the kinetic rate constant k can be summed from three mechanisms (Palandri and Kharaka, 2004), or

$$k = k_{25}^{nu} \exp\left[\frac{-E_a^{nu}}{R}\left(\frac{1}{T} - \frac{1}{298.15}\right)\right] +$$

$$k_{25}^{H} \exp\left[\frac{-E_a^{H}}{R}\left(\frac{1}{T} - \frac{1}{298.15}\right)\right] a_H^{n_H} + \qquad (A.2)$$

$$k_{25}^{OH} \exp\left[\frac{-E_a^{OH}}{R}\left(\frac{1}{T} - \frac{1}{298.15}\right)\right] a_{OH}^{n_{OH}}$$

where superscripts or subscripts nu, H, and OH indicate neutral, acid, and base mechanisms, respectively, E_a is the activation energy, k_{25} is the rate constant at 25°C, R is gas constant, T is absolute temperature, a is the activity of the species; and n is an exponent (constant). The rate constant k can be also dependent on other species such as Al^{3+} and Fe^{3+}. Two or more species may be involved in one mechanism. A general form of species dependent rate constants (extension of Equation A.2) is implemented in TOUGHREACT as

$$k = k_{25}^{nu} \exp\left[\frac{-E_a^{nu}}{R}\left(\frac{1}{T} - \frac{1}{298.15}\right)\right] +$$

$$\sum_i k_{25}^{i} \exp\left[\frac{-E_a^{i}}{R}\left(\frac{1}{T} - \frac{1}{298.15}\right)\right] \prod_j a_{ij}^{n_{ij}} \qquad (A.3)$$

where superscripts or subscripts i is the additional mechanism index, and j is species index involved in one mechanism that can be primary or secondary species. TOUGHREACT currently considers up to five additional mechanisms and up to five species involved in each mechanism.

Appendix B. Rate expression for Intra-aqueous kinetics and biodegradation

A general rate expression for intra-aqueous kinetic reaction and biodegradation has been incorporated into TOUGHREACT. Following the expression of Curtis (2003) and adding multiple mechanisms (or pathways), a general rate law used is:

$$r_i = \sum_{s=1}^{M} \begin{bmatrix} k_{i,s} & \text{rate constant} \\[2ex] \times \prod_{j=1}^{N_l} \left(\gamma_j^{v_{i,j}} C_j^{v_{i,j}} \right) & \text{product terms} \\[2ex] \times \prod_{k=1}^{N_m} \dfrac{C_{i,k}}{K_{Mi,k} + C_{i,k}} & \text{Monod terms} \\[2ex] \times \prod_{p=1}^{N_p} \dfrac{I_{i,p} + C_{i,p}}{I_{i,p}} & \text{inhibition terms} \end{bmatrix} \qquad (B.1)$$

where r_i is the reaction rate of the i-th reaction, M is the number of mechanisms or pathways, s is the mechanism counter, k is a rate constant, (often denoted v_{max}, maximum specific growth constant for biodegradation), γ_j is the activity coefficient of species j, C_j is the concentration of species j (with biodegradation, the product term is usually biomass concentration), $v_{i,j}$ is a stoichiometric coefficient, N_l is the number of reacting species in the forward rate term (called product terms), N_m is the number of Monod factors (Monod terms), $C_{i,k}$ is the concentration of the k-th Monod species, $C_{i,p}$ is the concentration of the p-th inhibiting species, $K_{Mi,k}$ is the k-th Monod half-saturation constant of the i-th species, N_P is the number of inhibition factors (inhibition terms), and $I_{i,p}$ is the p-th inhibition constant. Equation (B.1) accounts for multiple mechanisms and multiple products, Monod, and inhibition terms, which can cover many rate expressions

Appendix C. Parameters used for kinetic rate law

Calcite was assumed to react with aqueous species at local equilibrium because its reaction rate is typically quite rapid. Dissolution and precipitation of other minerals are kinetically-controlled. Kinetic rates are a product of the rate constant and reactive surface area (Eq. A.1 in Appendix A). Multiple mechanisms (including neutral, acid and base) are used for dissolution of minerals (Eqs. A.2 and A.3 in Appendix A). Kinetic parameters including rate constant (k_{25}), the activation energy (E_a), and the power term (n) for each mechanism are given in Table C.1. The thermodynamic data, kinetic parameters, and reactive surface areas used are discussed in Xu et al. (2007).

Table C.1. Parameters for calculating kinetic rate constants of minerals. Note that: (1) all rate constants are listed for dissolution; (2) A is specific surface area, k_{25} is kinetic constant at 25°C, E is activation energy, and n is the power term (Eq. A.2); (3) the power terms n for both acid and base mechanisms are with respect to H^+; (4) for pyrite, the neutral mechanism has n with respect to $O_2(aq)$, the acid mechanism has two species involved: one n with respect to H^+ and another n with respect to Fe^{3+}.

Mineral	A (cm^2/g)	Parameters for kinetic rate law							
		Neutral mechanism		Acid mechanism			Base mechanism		
		k_{25} $(mol/m^2/s)$	E_a (KJ/mol)	k_{25}	E_a	$n(H^+)$	k_{25}	E_a	$n(H^+)$
Calcite		At local equilibrium							
Quartz	9.1	1.0×10^{-14}	87.7						
Kaolinite	108.7	7.0×10^{-14}	22.2	4.9×10^{-12}	65.9	0.777	8.9×10^{-18}	17.9	-0.472
Illite	108.7	1.7×10^{-13}	35	1.0×10^{-11}	23.6	0.34	3.0×10^{-17}	58.9	-0.4
Oligoclase	9.1	1.4×10^{-12}	69.8	2.1×10^{-10}	65	0.457			
K-feldspar	9.1	3.9×10^{-13}	38	8.7×10^{-11}	51.7	0.5	6.3×10^{-22}	94.1	-0.823
Na-smectite	108.7	1.7×10^{-13}	35	1.0×10^{-11}	23.6	0.34	3.0×10^{-17}	58.9	-0.4
Chlorite	9.1	3.0×10^{-13}	88	7.8×10^{-12}	88	0.5			
Hematite	12.9	2.5×10^{-15}	66.2	4.1×10^{-10}	66.2	1			
Magnesite	9.1	4.6×10^{-10}	23.5	4.2×10^{-7}	14.4	1			
Dolomite	9.1	3.0×10^{-8}	52.2	6.5×10^{-4}	36.1	0.5			
Low-albite	9.1	2.8×10^{-13}	69.8	6.9×10^{-11}	65	0.457	2.5×10^{-16}	71	-0.572
Siderite	9.1	1.3×10^{-9}	62.76	6.5×10^{-4}	36.1	0.5			
Ankerite	9.1	1.3×10^{-9}	62.76	6.5×10^{-4}	36.1	0.5			
Dawsonite	9.1	1.3×10^{-9}	62.76	6.5×10^{-4}	36.1	0.5			
Ca-smectite	108.7	1.7×10^{-13}	35	1.0×10^{-11}	23.6	0.34	3.0×10^{-17}	58.9	-0.4
Alunite	9.1	1.0×10^{-12}	57.78				1.0×10^{-12}	7.5	-1.0
Pyrite	12.9	$k_{25}=2.8\times10^{-5}$ $E_a=56.9$ $n(O_2(aq))=0.5$		$k_{25}=3.0\times10^{-8}$ $E_a=56.9$ $n(H^+)=-0.5,$ $n(Fe^{3+})=0.5$					

REFERENCES

Balistrieri, L.S., 1998. Preliminary estimates of benthic fluxes of dissolved metals in Coeur d'Alene Lake, Idaho. Open File Report 98-793, U.S. Geological Survey, Seattle, WA, 40pp.

Curtis, G.P., 2003. Comparison of approaches for simulating reactive solute transport involving organic degradation reactions by multiple terminal electron acceptors. Computers & Geosciences 29, 319-329.

Doughty, C., Freifeld, B.M., Trautz, R.C., 2008. Site characterization for CO_2 geologic storage and vice versa – the Frio brine pilot, Texas, USA as a case study. Environmental Geology 54, 1635-1656.

Dzombak, D.A. Morel, F.M.M., 1990. Surface Complexation Modeling-Hydrous Ferric Oxide. John Wiley & Sons, New York, 393 pp.

Freifeld, B.M., Trautz, R.C., Kharaka, Y.K., Phelps, T.J., Myer, L.R., Hovorka, S.D., Collins, D.J., 2005. The U-tube: A novel system for acquiring borehole fluid samples from a deep geologic CO_2 sequestration experiment. Journal of Geophysical Research 110, B10203.

Gwo, J.P., Jardine, P.M., Wilson, G.V., Yeh, G.T.. 1996. Using a multiregion model to study the effects of advective and diffusive mass transfer on local physical nonequilibrium and solute mobility in a structured soil. Water Resource Research 32, 561-570.

Horowitz, A.J., Elrick, K.A., Robbins, J.A., Cook, R.B., 1995. Effect of mining and related activities on sediment trace element geochemistry of Lake Coeur D'Alene, Idaho, USA Part II: Subsurface sediments. Hydrological Process 9, 35-54.

Hovorka, S.D., Benson, S.M., Doughty, C.K., Freifeld, B.M., Sakurai, S., Daley, T.M., Kharaka, Y.K., Holtz, M.H., Trautz, R.C., Nance, H.S., Myer, L.R., Knauss, K.G., 2006. Measuring permanence of CO_2 storage in saline formations-The Frio experiment. Environmental Geosciences 13, 103–119.

Lasaga, A.C., Soler, J.M., Ganor, J., Burch, T.E., Nagy, K.L., 1994. Chemical weathering rate laws and global geochemical cycles. Geochimica et Cosmochimica Acta 58, 2361-2386.

Lichtner, P.C., 1988. The quasi-stationary state approximation to coupled mass transport and fluid-rock interaction in a porous medium. Geochimica et Cosmochimica Acta 52, 143-165.

Liger, E., Charlet L., Van Cappellen, P., 1999. Surface catalysis of U(VI) reduction by Fe(II). Geochimica et Cosmochimica Acta 63, 2939–2955.

Kuwabara, J.S., Carter, J.L., Topping, B.R., Fend, S.B., 2003. Importance of sediment-water interactions in Coeur d'Alene Lake, Idaho, USA: management implications. Environmental Management 32, 348-359.

Moberly, J.G., Borch T., Sani R.K., Spycher N.F., Şengör S.S., Ginn T.R., Peyton, B.M., 2009. Heavy metal-mineral associations in Coeur d'Alene river sediments: A synchrotron-based analysis. Water, Air, and Soil Pollution 200, 195-208.

Narasimhan, T.N., Witherspoon, P.A., 1976. An integrated finite difference method for analyzing fluid flow in porous media, Water Resources Research 12, 57–64.

Palandri, J., Kharaka, Y.K., 2004. A compilation of rate parameters of water-mineral interaction kinetics for application to geochemical modeling. Open File Report 2004-1068, U.S. Geological Survey, Menlo Park, CA, 64pp.

Parkhurst, D.L., Appelo, C.A.J., 1999. User's Guide to PHREEQC (Version 2) - A computer program for speciation, batch-reaction, one-dimensional transport, and inverse geochemical calculations. Water-Resources Investigations Report 99-4259, U.S. Geological Survey, Denver, CO. 312pp.

Pruess, K., 2004. The TOUGH codes: A family of simulation tools for multiphase flow and transport processes in permeable media. Vadose Zone Journal 3, 738-746.

Pruess, K., Spycher, N., 2007. ECO2N - A fluid property module for the TOUGH2 code for studies of CO_2 storage in saline aquifers. Energy Conversion and Management 48(6), 1761-1767.

Rickard, D., 1995. Kinetics of FeS precipitation: Par 1. Competing reaction mechanisms. Geochimica et Cosmochimica Acta 59, 4367-4379.

Şengör, S.S., Spycher, N.F., Ginn, T.R., Moberly, J., Peyton, B., Sani, R.K., 2007a. Reductive dissolution and metal transport in Lake Coeur d'Alene sediments, In: Bullen T., Wang Y., (eds.) Water-Rock Interaction, WRI-12, Taylor & Francis, New York, p. 895-899.

Şengör, S.S., Spycher, N.F., Ginn, T.R., Sani, R.K., Peyton, B., 2007b. Biogeochemical reactive-diffusive transport of heavy metals in Lake Coeur d'Alene sediments. Applied Geochemistry 22, 2569-2594.

Sonnenthal E., Ito, A., Spycher, N., Yui, M., Apps, J., Sugita, Y., Conrad, M., Kawakami, S., 2005. Approaches to modeling coupled thermal, hydrological, and chemical processes in the Drift Scale Heater Test at Yucca Mountain. International Journal of Rock Mechanics and Mining Sciences 42, 6987-719.

Spycher, N.F., Sonnenthal, E.L., Apps, J.A., 2003. Fluid flow and reactive transport around potential nuclear waste emplacement tunnels at Yucca Mountain, Nevada. Journal of Contaminant Hydrology 62-63, 653-673.

Steefel, C.I., MacQuarrie, K.T.B., 1996. Approaches to modeling of reactive transport in porous media, In: Lichtner, P.C., Steefel, C.I., Oelkers, E.H. (eds.), Reactive transport in porous media, Reviews in Mineralogy, Mineral Society of America 34, p. 83-129.

Toevs, G.R., Morra, M.J., Polizzotto, M.L., Strawn, D.G., Bostick, B.C., Fendorf, S., 2006. Metal(loid) diagenesis in mine-impacted sediments of Lake Coeur d'Alene, Idaho. Environmental Science and Technology 40, 2537–2543.

Van Cappellen, P., Gaillard, P., 1996. Biogeochemical dynamics in aquatic sediments, In: Lichtner, P.C., Steefel, C.I., Oelkers, E.H. (eds.) Reactive transport in porous media, Reviews in Mineralogy, Mineral Society of America 34, p. 335–376.

Van Genuchten, M. Th., 1980. A Closed-form equation for predicting the hydraulic conductivity of unsaturated soils. Journal of American Soil Science Society 44, 892 – 898.

Winowiecki, L., 2002. Geochemical cycling of heavy metals in the sediment of Lake Coeur d'Alene, Idaho. Masters Thesis, University of Idaho, Moscow, Idaho. 236pp.

Xu, T., 2008. Incorporation of aqueous reaction kinetics and biodegradation into TOUGHREACT: Application of a multi-region model to hydrobiogeochemical transport of denitrification and sulfate reduction. Vadose Zone Journal 7, 305-315.

Xu, T., Apps, J.A., Pruess, K., Yamamoto, H., 2007. Numerical modeling of injection and mineral trapping of CO_2 with H_2S and SO_2 in a sandstone formation. Chemical Geology 242, 319-346.

Xu, T., Pruess, K., 2001. Modeling multiphase non-isothermal fluid flow and reactive geochemical transport in variably saturated fractured rocks: 1. Methodology. American Journal of Science 301, 16-33.

Xu, T., Sonnenthal, E.L., Spycher, N., Pruess, K. 2006. TOURGHREACT: A simulation program for non-isothermal multiphase reactive geochemical transport in variably saturated geologic media. Computers & Geosciences 32, 145-165.

Yeh, G.T., Tripathi, V.S., 1991. A model for simulating transport of reactive multispecies components: model development and demonstration. Water Resources Research 27, 3075-3094.

Zhang, G., Spycher, N., Sonnenthal, E., Steefel, C., Xu, T., 2008. Modeling reactive multiphase flow and transport of concentrated aqueous solutions. Nuclear Technology 164, 180-195.

Zheng, L., Apps, J.A., Zhang, Y., Xu, T., Birkholzer, J., 2009. On mobilization of lead and arsenic in groundwater in response to CO_2 leakage from deep geological storage. Chemical Geology 268, 281-297.

Figure 1. Space discretization and geometric data for integral finite difference method.

Figure 1. Subgridding in method of "multiple interacting continua" (MINC).

Figure 2. Schematic representation of a multi-region model for resolving local diffusive transport.

Figure 3. Schematic representation of 2-D radial flow model for supercritical CO_2 injection into a sandstone formation.

Figure 4. Distribution of supercritical CO_2 gas phase saturation (Sg) at different times for 2-D radial model (depths appear in negative number, indicating the distance below the top of the model domain, or caprock).

Figure 5. Distribution of total dissolved CO_2 (mol/kg H_2O) and pH at different times for 2-D radial model.

Figure 6. Changes of volume fraction of siderite and ankerite after 1,000 years.

Figure 7. Distribution of porosity after 1,000 years.

Figure 8. Percentage of amounts of CO_2 trapped in different phases over time.

Figure 9. Conceptual 1D diffusive biogeochemical model (Sengör et al, 2007b)

Figure 10.   Concentrations of key parameters, redox species, and metals with depth from the top of the sediment column. Lines show computed values, symbols (Summer 2001: triangle symbols; Fall 2001: square symbols) are measured values by Winowiecki (2002), except for Cu (average over interval shown, from Sengör et al. 2007b).

Figure 11. Computed change in abundance of Fe minerals from the top of the sediment column. The reductive dissolution of ferrihydrite leads to an increase in Fe(II) (Figure 10) and subsequent FeS and siderite precipitation.

Table 1. Hydrogeological parameters for the 2-D radial CO_2 injection problem.

Aquifer thickness	40 m
Permeability (horizontal)	1.0×10^{-13} m^2
Permeability (vertical)	1.0×10^{-14} m^2
Porosity	0.3
Compressibility	4.5×10^{-10} Pa^{-1}
Temperature	75 ^{0}C
Pressure	200 bar
Salinity	0.06 (NaCl mass fraction)
CO_2 injection rate	20 kg/s
Relative permeability	
Liquid (van Genuchten, 1980): $$k_{rl} = \sqrt{S^*}\left\{1 - \left(1 - \left[S^*\right]^{1/m}\right)^m\right\}^2$$ irreducible water saturation exponent	$S^* = (S_l - S_{lr})/(1 - S_{lr})$ $S_{lr} = 0.30$ $m = 0.457$
Gas (Corey, 1954): $$k_{rg} = (1 - \widehat{S})^2(1 - \widehat{S}^2)$$ irreducible gas saturation	$\widehat{S} = \dfrac{(S_l - S_{lr})}{(S_l - S_{lr} - S_{gr})}$ $S_{gr} = 0.05$
Capillary pressure	
Van Genuchten (1980) $$P_{cap} = -P_0\left(\left[S^*\right]^{-1/m} - 1\right)^{1-m}$$ irreducible water saturation exponent strength coefficient	$S^* = (S_l - S_{lr})/(1 - S_{lr})$ $S_{lr} = 0.03$ $m = 0.457$ $P_0 = 19.61\,\text{kPa}$

Table 2. Initial mineral volume fractions and possible secondary mineral phases used in the simulations.

Mineral	Chemical formula	Volume percent	
		of solid	*of medium*
Primary:			
Quartz	SiO_2	58	40.6
Kaolinite	$Al_2Si_2O_5(OH)_4$	2.02	1.41
Calcite	$CaCO_3$	1.93	1.35
Illite	$K_{0.6}Mg_{0.25}Al_{1.8}(Al_{0.5}Si_{3.5}O_{10})(OH)_2$	1.0	0.7
Oligoclase	$Ca_{0.2}Na_{0.8}Al_{1.2}Si_{2.8}O_8$	19.8	13.86
K-feldspar	$KAlSi_3O_8$	8.2	5.74
Na-smectite	$Na_{0.290}Mg_{0.26}Al_{1.77}Si_{3.97}O_{10}(OH)_2$	4	2.8
Chlorite	$Mg_{2.5}Fe_{2.5}Al_2Si_3O_{10}(OH)_8$	4.55	3.19
Hematite	Fe_2O_3	0.5	0.35
Porosity		----	30
Secondary:			
Anhydrite	$CaSO_4$		
Magnesite	$MgCO_3$		
Dolomite	$CaMg(CO_3)_2$		
Low-albite	$NaAlSi_3O_8$		
Siderite	$FeCO_3$		
Ankerite	$CaMg_{0.3}Fe_{0.7}(CO_3)_2$		
Dawsonite	$NaAlCO_3(OH)_2$		
Ca-smectite	$Ca_{0.145}Mg_{0.26}Al_{1.77}Si_{3.97}O_{10}(OH)_2$		
Alunite	$KAl_3(OH)_6(SO_4)_2$		
Pyrite	FeS_2		

Table 3. Initial total dissolved component concentrations for reactive transport simulations. Iron is the sum of Fe^{2+}, Fe^{3+} and their related complexes. Carbon is the sum of $CO_2(aq)$, $CH_4(aq)$, and their related species such as HCO_3^- and acetic acid(aq). Sulfur is the sum of sulfate and sulfide species

Component	Concentration (mol/kg H_2O)
Ca^{2+}	6.6×10^{-2}
Mg^{2+}	2.2×10^{-2}
Na^+	1.35
K^+	4.53×10^{-3}
Iron	4.63×10^{-4}
$SiO_2(aq)$	2.50×10^{-4}
Carbon	5.04×10^{-2}
Sulfur	4.20×10^{-5}
Al^{3+}	1.56×10^{-8}
Cl^-	1.49
pH	6.7
Temperature	$75°C$

Table 4. Microbial reactions and rate laws (from Sengör et al., 2007a). See Table 5 for parameter values.

Microbially mediated reactions:

$CH_3COO^- + 2O_2 \rightarrow 2CO_3^{-2} + 3H^+$ $\qquad\qquad R_{O2}$

$CH_3COO^- + 1.6NO_3^- \rightarrow 2CO_3^{-2} + 0.8N_2 + 1.4H^+ + 0.8H_2O$ $\qquad R_{NO3}$

$CH_3COO^- + 8Fe^{+3} + 4H_2O \rightarrow 8Fe^{+2} + 2CO_3^{-2} + 11H^+$ $\qquad R_{Fe+3}$

$CH_3COO^- + SO_4^{-2} \rightarrow 2CO_3^{-2} + HS^- + 2H^+$ $\qquad\qquad R_{SO4-2}$

Kinetic rate laws:

$$R_{O2} = V_m^{O2} \frac{[O_2]}{[O_2] + K_s^{O2}}$$

$$R_{NO3} = V_m^{NO3} \frac{[NO_3]}{[NO_3] + K_s^{NO3}} \frac{K_{O2}^{in}}{K_{O2}^{in} + [O_2]}$$

$$R_{Fe+3}^{(*)} = V_m^{Fe} \frac{K_{O2}^{in}}{K_{O2}^{in} + [O_2]} \frac{K_{NO3}^{in}}{K_{NO3}^{in} + [NO_3]}$$

$$R_{SO4-2} = V_m^{SO4} \frac{[SO_4^{2}]}{[SO_4^{2}] + K_s^{SO4}} \frac{K_{O2}^{in}}{K_{O2}^{in} + [O_2]} \frac{K_{NO3}^{in}}{K_{NO3}^{in} + [NO_3]} \frac{K_{Fe}^{in}}{K_{Fe}^{in} + [Fe^{+3}]}$$

V_m^i Maximum substrate utilization rate constant
K_s^i Half saturation constant
K_i^{in} Inhibition constants
(*)   Assumes unlimited Fe^{+3} supply from abundant solid Fe hydroxides

Table 5. Values of parameters in Table 4 (from Sengör et al., 2007a, except for V_m^{Fe}). The value of V_m^{Fe} was recalibrated to take into account the effect Fe(II) sorption onto ferrihydrite, which was ignored in the original model.

Parameter (units)	Model Value
V_m^{O2} (s^{-1})	5×10^{-9}
V_m^{NO3} (s^{-1})	2×10^{-10}
V_m^{Fe} (s^{-1})	15×10^{-12}
V_m^{SO4} (s^{-1})	3×10^{-9}
K_s^{O2} (molal)	2.41×10^{-5}
K_s^{NO3} (molal)	1.13×10^{-4}
K_s^{SO4} (molal)	1×10^{-3}
K_{O2}^{in} (molal)	1.61×10^{-8}
K_{NO3}^{in} (molal)	1×10^{-7}
K_{Fe}^{in} (molal)	1×10^{-8}

Table 6. Minerals included in the simulation, and reaction constraints.

Mineral	Initial Amount (% Volume)	Constraint on reaction	$k \times A$ (mol s^{-1} kg^{-1}$_{water}$)
Ferrihydrite	1.4	Equilibrium	none
FeS	none	Equilibrium	none
Siderite	10	$R_{FeCO3} = kA(Q/K-1)$	5 x 10^{-14}
Sphalerite[1]	none	$R_{ZnS} = kA[Zn^{+2}][H_2S](Q/K-1)^{0.01}$	2.7 x 10^{-3}
Galena[1]	none	$R_{PbS} = kA[Pb^{+2}][H_2S](Q/K-1)^{0.01}$	2.7 x 10^{-3}
Chalcocite[1]	none	$R_{Cu2S} = kA[Cu^{+}][H_2S](Q/K-1)^{0.01}$	2.7 x 10^{-3}

For each mineral, k and A represent the rate constant and reactive surface area, respectively, and Q and K represent the activity product and solubility product, respectively. Values of $k \times A$ were roughly calibrated, and intentionally kept low for heavy metal sulfides, which are only used here as "proxies" for precipitation in various sulfide forms. The form of the rate law for sulfides is after Rickard (1995), except for the $(1- Q/K)$ term, which was added to ensure the rate convergence to zero at equilibrium. The small exponent on this term is meant to keep it near 1 except at equilibrium when this term drops to 0.

Table 7. Input water composition (oxic lake water, from Sengör et al., 2007a)

Component	Concentration	Units
pH (25°C)	7.2	
Cl	1.95×10^{-5}	molal
CO$_{3(tot)}$	3.54×10^{-4}	molal
SO$_4$	5.83×10^{-5}	molal
Ca	1.37×10^{-4}	molal
Mg	8.64×10^{-5}	molal
Na	1.00×10^{-4}	molal
K	1.28×10^{-5}	molal
NO$_3$	8.00×10^{-5}	molal
O$_{2(aq)}$	4.25×10^{-4}	molal
Fe	3.11×10^{-9}	molal
Pb	5.31×10^{-8}	molal
Zn	8.72×10^{-6}	molal
Cu	1.18×10^{-8}	molal
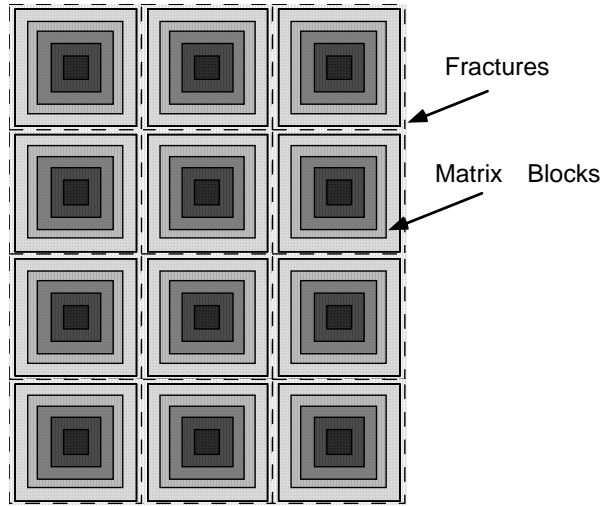
Figure 1. Subgridding in method of "multiple interacting continua" (MINC).
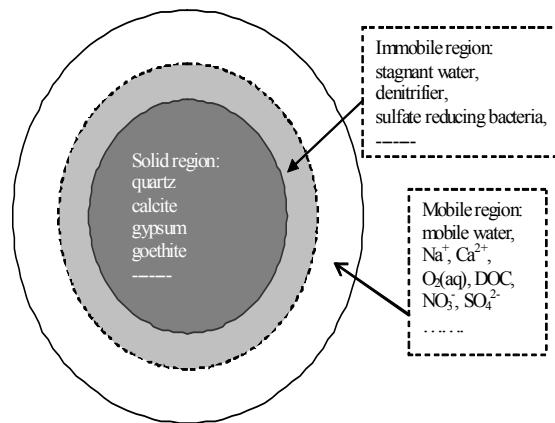
Figure 2. Schematic representation of a multi-region model for resolving local diffusive transport.
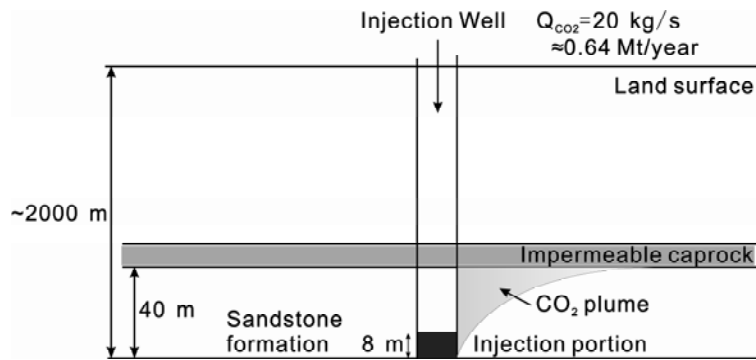
Figure 3. Schematic representation of 2-D radial flow model for supercritical CO_2 injection into a sandstone formation.
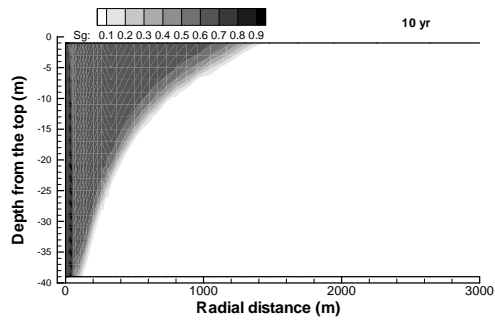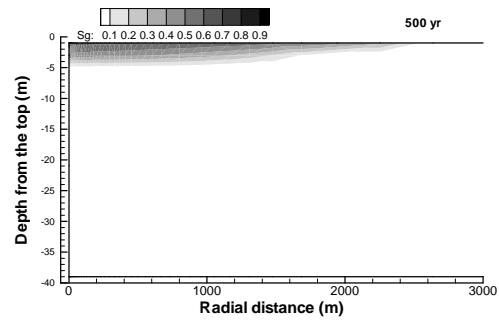
(a) 10 years   (b) 100 years

Figure 4. Distribution of supercritical CO_2 gas phase saturation (Sg) at different times for 2-D radial model (depths appear in negative number, indicating the distance below the top of the model domain, or caprock).
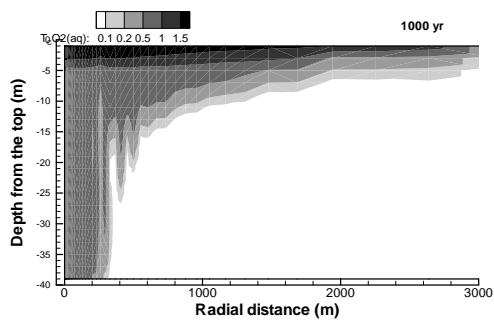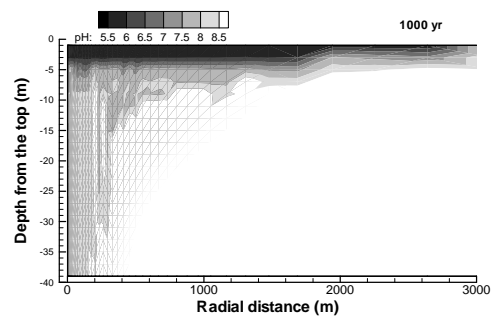
(a) Dissolved CO_2 (b) pH

Figure 5. Distribution of total dissolved CO_2 (mol/kg H_2O) and pH at different times for 2-D radial model.
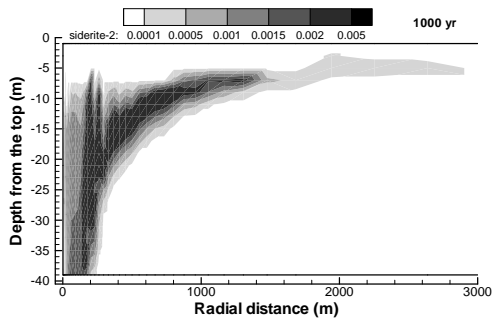
(a) Siderite

(b) Ankerite

Figure 6. Changes of volume fraction of siderite and ankerite after 1,000 years.

Figure 7. Distribution of porosity after 1,000 years.

33

Figure 8. Percentage of amounts of CO_2 trapped in different phases over time.

Figure 9. Conceptual 1D diffusive biogeochemical model (Sengor et al, 2007b)

Figure 10.   Concentrations of key parameters, redox species, and metals with depth from the top of the sediment column. Lines show computed values, symbols (Summer 2001: triangle symbols; Fall 2001: square symbols) are measured values by Winowiecki (2002), except for Cu (average over interval shown, from Sengor et al. 2007b).

Figure 11. Computed change in abundance of Fe minerals from the top of the sediment column. The reductive dissolution of ferrihydrite leads to an increase in Fe(II) (Figure 10) and subsequent FeS and siderite precipitation.

DISCLAIMER